

1 Evaluation of a reduced pressure chemical ion reactor utilizing
2 adduct ionization for the detection of gaseous organic and
3 inorganic species

4

5 Matthieu Riva^{1,2, †,*}, Veronika Pospisilova^{1,†}, Carla Frege¹, Sebastien Perrier², Priyanka Bansal¹,
6 Spiro Jorga¹, Patrick Sturm¹, Joel A. Thornton³, Urs Rohner¹, Felipe Lopez-Hilfiker^{1,*}

7 ¹ TOFWERK, 3645 Thun, Switzerland

8 ² Université Claude Bernard Lyon 1 CNRS, IRCELYON 69626, Villeurbanne France

9 ³ Department of Atmospheric Sciences, University of Washington, Seattle, Washington 98195,
10 USA.

11

12 *Correspondence to:* matthieu.riva@tofwerk.com & lopez@tofwerk.com

13 † These authors contributed equally.

14

15

16

17

18 **Abstract**

19 Volatile organic compounds (VOCs) and volatile inorganic compounds (VICs) provide critical information
20 across many scientific fields including atmospheric chemistry, soil, and biological processes. Chemical
21 ionization (CI) mass spectrometry has become a powerful tool for tracking these chemically complex and
22 temporally variable compounds in a variety of laboratory and field environments. It is particularly powerful
23 with time-of-flight mass spectrometers, which can measure hundreds of compounds in a fraction of a second
24 and have enabled entirely new branches of VOC/VIC research in atmospheric and biological chemistry. To
25 accurately describe each step of these chemical, physical, and biological processes, measurements across
26 the entire range of gaseous products is crucial. Recently, chemically comprehensive gas-phase
27 measurements have been performed using many CI mass spectrometers deployed in parallel, each utilizing
28 a different ionization method to cover a broad range of compounds. Here we introduce the recently
29 developed Vocus AIM (Adduct Ionization Mechanism) ion-molecule reactor (IMR), which samples trace
30 vapors in air and ionizes them via chemical ionization at medium pressures. The Vocus AIM supports the
31 use of many different reagent ions of positive and negative polarity and is largely independent of changes
32 in the sample humidity. Within the present study, we present the performance and explore the capabilities
33 of the Vocus AIM using various chemical ionization schemes, including Chloride (Cl^-), Bromide (Br^-),
34 Iodide (I^-), Nitrate (NO_3^-), Benzene cations (C_6H_6^+), Acetone dimers ($(\text{C}_3\text{H}_6\text{O})_2\text{H}^+$), and Ammonium
35 (NH_4^+) reagent ions primarily in laboratory and flow tube experiments. We report the technical
36 characteristics, operational principles, and compare its performance in terms of time response, humidity
37 dependence, and sensitivity to that of previous chemical ionization approaches. This work demonstrates the
38 benefits of the Vocus AIM reactor which provides a versatile platform to characterize VOCs and VICs in
39 real time at trace concentrations.

40

41 **1. Introduction**

42 Mass spectrometry represents a nearly universal method for determining the chemical composition of
43 organic and inorganic species across various environmental matrices. In the fields of environmental and
44 atmospheric chemistry, chemical ionization (CI) is a versatile real-time method to measure individual
45 organic and inorganic compounds in air at trace concentrations (Yuan et al., 2017; Riva et al., 2019; Zhang
46 W. et al., 2023; Zhang Y. et al., 2023). As in all chemical ionization systems, trace analytes in air react with
47 excess reagent ions, leading to the formation of charged product ions usually via electron/proton transfer
48 or adduct formation (Zhang W. et al., 2023; Zhang Y. et al., 2023). Advances in the field of chemical
49 ionization over the last decade have yielded exceptionally low detection limits down to 10^4 molecules cm^{-3}
50 (part-per-quadrillion), expanded dynamic ranges, and the capability of measuring a wide range of gaseous
51 organic and inorganic species with time resolutions of up to 50 Hz (Riva et al., 2019; Zhang W. et al., 2023;
52 Zhang Y. et al., 2023).

53 Chemical ionization mass spectrometers are uniquely able to measure temporal variability of trace
54 VOC and atmospheric oxidation products; both in the laboratory and in the field, providing a critical tool
55 to mechanistically track the most important atmospheric oxidation processes (Hallquist et al., 2009, Ehn et
56 al., 2014, Bianchi et al., 2019). In particular, CI has made enormous improvements in the detection and
57 quantification of reactive gaseous oxygenated species, including peroxy (RO_2) radicals, stabilized Criegee
58 intermediates, and inorganic acids and bases which are difficult to directly detect with any other available
59 analytical technique (Berndt et al., 2015, 2017, 2018; Breitenlechner et al., 2017; Hansel et al., 2018;
60 Krechmer et al., 2018). For example, measurements via chemical ionization mass spectrometry (CIMS)
61 have been pivotal in discovering the existence and importance of extremely low volatility organic molecules
62 (ELVOCs). These compounds are now understood to be formed ubiquitously in the atmosphere and are
63 critical to new particle formation and growth (Ehn et al., 2014; Bianchi et al., 2019). As a result, CIMS has
64 emerged as a core analytical tool in atmospheric chemistry and related fields which require high sensitivity,
65 high temporal resolution, and molecular-level speciation (Bruderer et al., 2019; Riva et al., 2019; Tang et
66 al., 2019; Mazzucotelli et al., 2022; Zhang W. et al., 2023; Zhang Y. et al., 2023).

67 With the right selection of reagent ions, CI offers the possibility of soft, selective, and sensitive
68 online detection, for essentially any class of chemical compounds. While in practice, no reagent ion can
69 simultaneously detect the entire distribution of volatile compounds present in the atmosphere with sufficient
70 selectivity and sensitivity, different reagent ions can be selected to target distinct chemical families
71 (Crouse et al., 2006; Bertram et al., 2011, 2016; Lee et al., 2014, Bianchi et al., 2019, Riva et al., 2019;
72 Zhang W. et al., 2023; Zhang Y. et al., 2023). Therefore, a critical choice for chemical ionization operators
73 is which reagent ion is best suited to measure compounds of interest in each measurement scenario.

74 Recent advancements in the design of the reactor have sought to improve measurement quality by
75 addressing two outstanding limitations of chemical ionization mass spectrometers: (i) improved detection
76 efficiency by refining the reactor geometry and optimizing the flow dynamics within the system, and (ii)
77 reliable, reproducible, and fully controlled reaction conditions. Improvements in the detection efficiency
78 depend on the balance of two critical parameters in any chemical ionization reactor. First, compounds
79 present in the sample gas stream need to be efficiently transported to the reaction cell and mix/react with
80 the reagent ions. The efficiency of the first step depends primarily on ionization pressure and absolute flow
81 rate (i.e., residence time). At atmospheric pressure, gases diffuse slowly, and maintaining laminar flows
82 between the sample line and reaction cell is straightforward (e.g., Eisele-inlet, MION, Crossflow CIMS)
83 (Eisele and Tanner, 1993; Palm et al., 2019; Rissanen et al., 2019, Pfeifer et al., 2020). However, operating
84 at high pressure makes controlling ionization conditions much more challenging. Therefore, most CIMS
85 instruments operated at a reduced pressure to facilitate control of the ionization conditions. Sample vapors
86 enter most reduced-pressure chemical ionization mass spectrometers through a critical orifice, which
87 introduces turbulence as the gas expands into the reaction cell. These turbulences can introduce contact
88 between the neutral sample gas and the reactor walls, resulting in memory effects and losses of reactive
89 trace compounds by collision with the walls. While there have been numerous efforts to improve the
90 introduction of sample gases into reduced pressure reactors by laminarizing (Palm et al., 2019) the incoming
91 airflow or controlling the expansion inside of specially coated glass tubes (Vasquez et al., 2018), these
92 approaches are often complex and demand considerable optimization, which has hindered their widespread

93 adoption. Consequently, turbulent wall losses and memory effects continue to pose substantial challenges
94 in reduced-pressure chemical ionization instruments, particularly when detecting reactive or sticky
95 compounds.

96 Operating chemical ionization instruments at reduced pressure provides more refined control over
97 ion chemistry since it allows for more straightforward and effective manipulation of ions within the
98 instrument. Of particular nuisance in nearly all chemical ionization approaches is water vapor, which is
99 highly variable and can have significant effects on the chemical ionization process. The formation of water
100 clusters, which grow rapidly as a function of increasing pressure, presents a specific challenge for
101 measurements taken near atmospheric pressure. Even chemical ionization approaches that operate at low
102 pressures like proton transfer reaction (PTR) can be affected by the presence of water vapor (Yuan et al.,
103 2017). PTR instruments are widely used for the detection of trace VOC using high electric fields to control
104 the reagent ion populations under changing humidity. While PTR instruments can largely control the
105 ionization and collision conditions in the reactor, applying high electric fields results in extensive
106 fragmentation of some critical functional groups in many fields (Yuan et al., 2017). Further, the PTR
107 ionization process is well known to lead to significant fragmentation of labile compounds such as acids,
108 peroxides, and alcohols. The fragmentation induced by protonation or charge transfer reactions along with
109 elevated collision energy within the reactor significantly complicates the mass spectrum, in some cases
110 limiting the possibility of retrieving the accurate concentration and composition of many classes of
111 compounds including highly oxygenated and functionalized organic species.

112 To improve the sensitivity (specificity) and reduce the degree of fragmentation, softer chemical
113 ionization techniques relying on adduct formation have become increasingly popular, especially when
114 molecular identification and mechanistic pathways must be accurately tracked. These reactors operate under
115 low ($E/N < 10$ Td) or field-free conditions at pressures (typically 50-500 mbar), to promote adduct formation
116 and stabilization (Zhang W. et al., 2023; Zhang Y. et al., 2023). Fluid dynamics and the degree of turbulence
117 inside the reactor govern reaction times and ion transport in such reactors. At these elevated ionization
118 pressures, the effect of water vapor can become a critical parameter affecting sensitivity. Routinely used

119 reagent ions can result in order of magnitude changes in sensitivity under atmospherically relevant
120 fluctuations of humidity (Lee et al., 2014; Breitenlechner et al., 2017; Zhang W. et al., 2023; Zhang Y. et
121 al., 2023). Correcting the data for each compound's humidity dependence is an error-prone and time-
122 consuming process where each compound must be treated essentially individually. Flooding the reactor
123 with water vapor, as done in techniques like Vocus PTR, can suppress the humidity dependence of some
124 compounds. Such approaches are only applicable to certain groups of compounds whose water vapor
125 dependence becomes weaker at higher absolute concentrations of water, which is not a universal
126 characteristic. In general, the lack of adequate water vapor control remains a major drawback of chemical
127 ionization systems most critically those operated at pressures greater than 10 mbar.

128 Herein we introduce the Vocus AIM ion molecule reactor (IMR) and report the technical
129 characteristics, operation principle, and performance of this new chemical reactor. We evaluate its
130 performance by reporting the time response of nitric acid, demonstrating a novel approach to suppress
131 humidity dependence, and comparing sensitivity to other CI reactors. We present the design and capabilities
132 of the Vocus AIM using a wide variety of reagent ions, including Chloride (Cl^-), Bromide (Br^-), Iodide (I^-),
133 Nitrate (NO_3^-), Benzene cations (C_6H_6^+), Acetone dimers ($(\text{C}_2\text{H}_5\text{O})_2\text{H}^+$), and Ammonium (NH_4^+) ions.
134 Finally, we show the measurement of RO_2 radicals and oxygenated VOCs acquired during the proof-of-
135 concept experiment of OH/O_3 -initiated oxidation of α -pinene. This work highlights the benefits of the
136 Vocus AIM reactor within atmospheric chemistry and its limitations.

137 **2. Experimental Section**

138 **2.1. Vocus AIM Reactor Design**

139 Medium pressure chemical ionization (20-500 mbar) systems are typically designed as flow tube reactors
140 which primarily transport ions toward the reactor exit by gas flow. Manipulating ions at high pressure would
141 require high electric fields which are either impractical or could fragment the labile analyte ions. Further,
142 RF devices that could focus ions into a beam, do not efficiently operate at such high pressures, precluding
143 their efficient use. Therefore, the Vocus AIM reactor operates on many of the same fundamental principles

144 of more traditional flow tube reactors, including field-free ionization conditions (Figure 1) and fluid
145 dynamic transport of ions through the reactor. Specifically, the new design includes improvements in
146 sample and reagent ion introduction, a conductive polytetrafluoroethylene (cPTFE) Teflon conical reaction
147 chamber to improve time response, and a simple yet efficient quadrupole based differentially pumped TOF
148 interface.

149 Gases enter the reactor manifold via a ½" O.D. Swagelok fitting which is pumped through an inlet
150 via a radially symmetric pump port. Excess flow is used to maintain short residence time and to minimize
151 inlet memory effects such as surface reaction (conversion) and irreversible wall losses. Typical make-up
152 flow rates of 5-10 standard liters per minute (slpm) are used to transport neutral analytes efficiently to the
153 entrance of the reactor. A bored through Swagelok interface ensures that all wetted surfaces before the
154 reactor are Teflon®, to minimize the retention and memory of the inlet line for semi-volatile gases and
155 reduce surface activity. At the entrance of the Vocus AIM IMR, the sample flow enters directly into the
156 center of the conical reactor at a flow rate of 1.8 slpm through a stainless-steel critical orifice (0.475 mm)
157 and a PFA Teflon® sample flow guide which promotes subsampling from the center of the laminar inlet
158 flow. The reactor is typically operated at a pressure of 50 mbar as a compromise between sensitivity and
159 linear range and is controlled by a pressure control valve and an IDP3 vacuum pump (Agilent Technologies,
160 IDP3). The reactor is temperature controlled to 50 °C, which is the lowest temperature that can be reliably
161 controlled across various field conditions to ensure constant reaction conditions. While a lower reactor
162 temperature would promote adduct formation, the long-term stability of thermal conditions would be more
163 difficult to maintain. Reagent ions are generated by compact Vacuum Ultra-Violet (VUV) ion sources
164 arranged radially around the central axis with reactant ions injected at an angle (45 degrees) to intersect the
165 expanding sample flow with minimal sample deflection and ensure that no VUV light directly enters the
166 IMR. Each ion source introduces the ions into the reactor with a standard flow rate of 0.25 slpm for optimum
167 reagent ion yield (Figure S1), nearly an order of magnitude lower flows than polonium or X-ray based ion
168 sources typically used. The residence time inside the reactor under these standard conditions is ~ 10 ms.

169 Modeled flow velocities in the Vocus AIM IMR (Figure 1) were used to optimize the flow patterns
170 inside the reaction cell. The velocity field shows the intersection of the reagent ion jet with the sample flow
171 and was optimized to minimize the contact of sample gas with reactor surfaces as well as to prevent
172 turbulent eddies near the gas expansion region. The gas flow dynamics were modeled with the open-source
173 computational fluid dynamics (CFD) software OpenFOAM v8 (<https://openfoam.org/>) using a customized
174 solver (<https://github.com/pasturm/rhoReactingPimpleFoam>) to simulate supersonic flow in a vacuum with
175 mixing of different gases. The final geometry is constrained by machinability (finite tool dimensions) while
176 also minimizing the response time and reducing reactive and ion wall losses.

177 2.2 Reagent Ion Generation

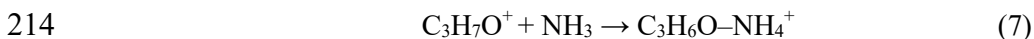
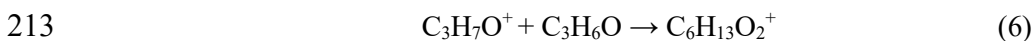
178 Compact VUV ion sources generate reagent ions by converting photons from a VUV lamp (UV Lamp
179 Krypton DC PID PKS 106, Hereaus) at two wavelength bands corresponding to energies of ~10.0 and 10.6
180 eV into the desired reagent ions (Ji et al., 2020; Breitenlechner et al., 2022). As in prior work, we utilize a
181 primary photo-absorber (e.g., benzene) as a source of photoelectrons and directly formed cations to generate
182 subsequent reagent ions. Permeation tubes are held at 80 °C in a compact oven and deliver constant amounts
183 of corresponding photo-absorber and reagent ion precursor into the 0.250 slpm UHP nitrogen stream.
184 Gaseous benzene (C₆H₆, Sigma Aldrich, ≥99.9%) delivered from the permeation tube, enters the VUV lamp
185 housing and is photoionized (with an absorption cross-section of 4 x10¹⁷ cm² molecule⁻¹ and ionization
186 potential = 9.24 eV), yielding C₆H₆⁺ and photoelectrons (Lavi et al., 2018). By mixing benzene with trace
187 methyl iodide (CH₃I, Sigma Aldrich, 99.8%), bromoethane (C₂H₅Br, Sigma Aldrich, ≥99%) or nitric acid
188 (HNO₃, Sigma Aldrich, ≥65.6%), various anions such as I⁻, Br⁻, or NO₃⁻ are generated alongside with C₆H₆⁺
189 following reactions equations (1 and 2) and are introduced into the Vocus AIM reactor. **The compatibility**
190 **between multiple ion chemistries in the AIM system is determined by whether a generated reagent ion can**
191 **detect the neutral precursors from any other attached ion source.** A small aperture at the exit of the
192 illuminated region of the ion source prevents back-diffusion of sample air into the primary ionization
193 chamber.



196 By manipulating the above mechanisms, other reagent ions can be readily produced in high abundance and
197 high purity. Cl^- reagent ions can also be produced by introducing 0.250 slpm of UHP nitrogen through the
198 permeation tube oven containing pure dichloromethane (CH_2Cl_2 , Sigma Aldrich, $\geq 99.8\%$) permeation tube.
199 Once formed, anion reagent ions mix with the sample flow in the main reaction chamber and ionize the
200 compounds of interest (M) through the reactions described in equations (3 and 4), with X being I^- , Br^- , Cl^-
201 or $(\text{HNO}_3)_n\text{NO}_3^-$ ($n = 0, 1, 2$).



204 To generate ammonium ions, we irradiate gaseous acetone with VUV light, which results in self-protonated
205 acetone (5) and directly reacts with the acetone molecules yielding protonated acetone dimers (6) (Dong et
206 al., 2022). A continuous flow of NH_3 , typically a few sccm, (i.e., $[\text{NH}_3] > 100$ ppm) from a 1% gas cylinder
207 (in nitrogen) can be introduced directly into the VUV source along with the acetone (Figure 1), NH_3
208 molecules react with the protonated acetone yielding acetone-ammonia adducts which can be used for
209 subsequent ionization in the main reaction chamber (7). **If the concentration of NH_3 is lower than 100 ppm,**
210 **multiple ionization processes might occur (e.g., acetone dimers, charge transfer,...) which would**
211 **complicate the mass spectrum analyses.**



215 Similar to anion reagent ions, these positive ions can ionize the compounds of interest through either adduct
216 formation or proton transfer or in the case of benzene, charge transfer. At pressures of 50 mbar, most
217 chemical ionization reactions occur via ligand switching reactions involving the analyte and hydrated
218 reagent ions.

219 To minimize the effect of water vapor during the ionization process inside the IMR, a water vapor
220 control system consisting of a regulated flow of a dopant (i.e., organic compound) can be injected directly
221 into the IMR (Figure 1). By replacing water with a stable concentration of the dopant, a stable ion
222 distribution is obtained across the entire range of relative humidity (RH) (further discussed in section 3.2).

223 2.4 Vacuum Interface and Analyzer

224 At the exit of the Vocus AIM reactor, product ions are sampled through a 1 mm orifice into the differentially
225 pumped vacuum interface. The efficiency with which the ions at the end of the reactor are sampled depends
226 primarily on the ratio of the sample flow which exits through the orifice relative to the flow towards the
227 vacuum pump evacuating the reaction chamber. This flow split is in turn also dependent on the reactor
228 pressure but is typically ~ 0.5 slpm. After entering the next stage of the interface, an RF-only quadrupole
229 ion guide efficiently focuses the analyte ions into a narrow beam, leading to the net removal of the neutral
230 molecules by a vacuum pump (Ebara PDV 500). Typical RF amplitudes of $100 V_{p-p}$ are sufficient to focus
231 most ions without significant ion activation for the iodide-water adduct where the iodide-water adduct is a
232 very weakly bound complex that is known to respond to transfer through vacuum interfaces relative to its
233 known thermodynamic distribution. In general, reagent ions and analyte ions that are very weakly bound
234 to the reagent ions (e.g., water cluster with a binding energy of 10 kcal/mol) (Caldwell et al., 1989) are
235 often observed to deviate from the thermodynamic distribution with RF amplitudes $>50 V_{p-p}$. This is not
236 entirely problematic, as the binding energy of these complexes is usually too weak for sensitive detection
237 even at the weakest transfer conditions. For typical analytes with moderate binding energies (e.g., iodide-
238 formic acid adducts), no significant declustering is observed at RF amplitudes $<125 V_{p-p}$. We find that the
239 optimal voltage gradients in the first quadrupole region are typically all 0 V between electrodes, as ions are
240 focused on the radial direction efficiently by the RF but transported axially by the gas flow. This ensures
241 that ions are transmitted with the lowest possible added energy into the next stage of the vacuum interface.
242 The rest of the differentially pumped interface is pumped by a single split flow turbo pump (Pfeiffer SF270)
243 and consists of an additional segmented quadrupole ion guide held at 10^{-2} mbar which transfers

244 energetically cooled ions into a lens stack held at 10^{-5} mbar before an orthogonal extraction in a time-of-
245 flight mass analyzer (Tofwerk Vocus CI-TOF 2R) operated at $<10^{-6}$ mbar. The instrument was configured
246 to measure a mass-to-charge (m/Q) range of 1–900 Th (12 kHz extraction frequency) with a mass resolving
247 power of 10 000 – 11 000 for the experiments described herein.

248 2.5 Flow Tube Oxidation Experiments

249 Ozonolysis/OH radical initiated oxidation of α -pinene ($C_{10}H_{16}$) experiments were performed under dry
250 conditions, at room temperature and atmospheric pressure in a flow tube reactor. The reactor consisted of
251 a ~ 6-litre Pyrex glass tube (80 mm i.d., \times 120 cm length). The total flow rate of dry synthetic air (N_2/O_2
252 80:20) was set at 5.5 slpm giving an average residence time of 70 seconds. Mixing ratio of 60 -70 ppb of
253 ozone generated by an ozone generator (Fisher Scientific, SOG-1) was continuously injected into the flow
254 tube. A mixing ratio of 200 ppb α -pinene was introduced from a homemade gas cylinder (40 ppm in UHP
255 N_2). The sample was immediately sampled into the reactor at a sample flow rate of 1.8 slpm with the excess
256 flow going to exhaust.

257 2.6 Calibration

258 To measure the instrument's sensitivity, we calibrated the reactor using different compounds each selected
259 to follow general structural selectivity rules for each ion chemistry. For example, no sensitivity for xylene
260 is reported for negative ions, as negative ions like iodide do not detect xylene with any significant
261 sensitivity. To calibrate benzene cations, we used a multicomponent gas (Apel Riemer Environmental Inc)
262 containing a mixture of hydrocarbons and ketones (Table S1). An internal calibration gas system consisting
263 of two mass flow controllers (Bronkhorst, capacity 30 and 2000 sccm) and a mixing volume diluted a flow
264 of 10 sccm of the gas standard into a carrier flow of 2000 sccm of UHP nitrogen resulting in a final mixing
265 ratio for each compound present in the gas mixture of 5 ppb. For iodide anions and protonated acetone
266 dimers, a liquid calibration system (LCS v2, Tofwerk) was used to form standard concentrations of lower
267 volatile species not compatible with gas cylinders. By introducing a continuous flow of liquid with known
268 concentration into a nebulizer and aluminum evaporation chamber, the LCS provides a continuous,

269 calibrated gas-phase concentration to the instrument. The evaporation chamber of the LCS was set to a
270 temperature of 150 °C, with a UHP nitrogen flow rate of 2000 **sccm** thereby slightly overflowing the sample
271 inlet. For the lower volatility compounds, we cannot rule out losses in the LCS, but find that collision-
272 limited sensitivities between positive and negative ion modes agree well within experimental uncertainty.
273 Aqueous solutions with concentrations ranging from 5 to 50 μM , and liquid flow rates of 10 $\mu\text{L}/\text{min}$, were
274 used to reach target concentrations in the low ppb range for each molecule and maintain constant water
275 vapor concentrations during calibration. Ammonia concentrations were generated using a gas standard and
276 independently compared to a cavity ring-down spectroscopy gas analyzer (Picarro Model G2508) to
277 validate the sensitivity and linearity of protonated acetone dimers towards ammonia (Figure S2).

278 Instrument backgrounds and detection limits are determined by measuring UHP nitrogen at the entrance
279 of the reactor. We note that measuring the total background should include any background measurement
280 of sampling inlets, but such characterization and best practices for sampling is beyond the scope of this
281 paper and discussed in detail elsewhere (Palm et al., 2019; Riva et al., 2019). We therefore report detection
282 limits using UHP nitrogen overflowing the inlet by using the zero port which introduces zero gas just to the
283 high-pressure (atmosphere) side of the critical orifice at the entrance of the reactor. We purged the
284 instrument before and after the calibration experiment for ten minutes with UHP nitrogen to determine the
285 instrument background count rates. As reported in detail previously (Palm et al., 2019), during a background
286 measurement the reactor walls are pushed out of equilibrium by the incoming clean air. This perturbation
287 can impart a transient effect on different compounds depending on primarily volatility. For volatile and
288 extremely low volatile compounds the response to a step change in concentration (introduction of zero air)
289 is close to instantaneous (< 100 ms) due to negligible adsorption (sticking rate), for the volatile species and
290 effectively infinitely slow evaporation rates from walls for the lowest volatility compounds (irreversible
291 loss). For background determinations the most challenging group of compounds are intermediate and semi-
292 volatile compounds which readily respond to changing inlet conditions and partition back and forth between
293 the reactor walls and the reactor flow. In laboratory conditions or at ground sites where temporal changes
294 are often only slowly changing, we use dry UHP N_2 to replace the incoming sample air for 1 minute. As

295 noted in prior work, under more dynamic environments the duration and frequency of instrument
296 background measurements should be decreased and increased respectively to match the temporal changes
297 which are to be measured.

298 **3. Results and discussion**

299 3.1. Vocus AIM time response

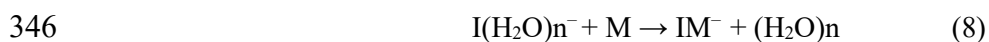
300 Real time measurements require fast time response to report temporal trends in measured concentrations
301 accurately. For many compounds, the time response can approach that of the volumetric time response of
302 the reactor (3 ~ 30 ms), however for semi-volatile (i.e., sticky) compounds the time response is often
303 observed to be much slower than the volumetric time constant as interaction with the reactor walls results
304 in smearing of the concentration over time. The primary interaction of the analyte and the reactor walls
305 defines the response time at constant temperature, pressure, and flow. Therefore, optimizing the shape and
306 the materials of the wetted surfaces is critical to maintaining a fast response. The Vocus AIM reactors'
307 conical design notably improves the time response by ensuring that the walls get further and further from
308 the exit orifice along the length of the reactor. This shape increases the probability that vapors that have
309 interacted with the wall are pumped away instead of being ionized and transferred into the mass analyzer.
310 It also ensures that in the region of the primary expansion, the recirculation eddies do not have significant
311 space to form, allowing a faster equilibration time at the entrance of the reactor (Figure 1). To accurately
312 measure dynamic changes in concentration, particularly for low-volatility species like oxidized organics,
313 inorganic acids, and reactive species, cPTFE is chosen as the reactor wall material. Teflon® based materials
314 have on average the weakest interaction with most organic and inorganic compounds (Morris et al., 2023)
315 and are therefore a good choice for the reactor walls. cPTFE in particular is chosen as its conductivity
316 prevents surface charge-up of the reactor walls which would result in unstable or slowly equilibrating ion
317 signals. We evaluate the performance of the reactor using molecules that represent a worst-case scenario
318 i.e., have a high surface affinity and interact strongly with the walls of the reactor. In Figure 2 we compare
319 the measurement of nitric acid in the AIM reactor with iodide adduct ionization with other IMR reactors

320 (Lee et al., 2018; Palm et al., 2019) with different approaches to improve the time response, notably a very
321 short stainless steel tubular reactor, and a larger flow tube reactor with laminarizer and sheath flow operated
322 at reduced pressure. To quantitatively compare the time responses of these different reactors we measured
323 the decay time, defined as the duration for the signal to fall below 90% of its peak value after the source of
324 nitric acid is removed. While the response time of the Vocus AIM reactor is not instantaneous, it is roughly
325 a factor of 3-4 faster than previously published medium pressure reactors. The improved time response is
326 most critical for ensuring that the memory effect in the reactor is minimized, crucial for applications where
327 fast transients need to be quantified, for example in mobile laboratories, aircraft, or flow tube reactors.

328 3.2 Water Vapor Control and Suppression.

329 A major limitation of chemical ionization reactors operated at elevated pressure is that water vapor can
330 strongly impact the net reaction mechanism and reagent ion distribution resulting in sensitivities that are
331 humidity-dependent (Zhang W. et al., 2023; Zhang Y. et al., 2023) as shown in Figure S3 for the reagent
332 ion distribution. Such changes pose considerable challenges for accurate quantification of species in
333 conditions where humidity is variable. The sensitivity to a given compound will depend on whether water
334 vapor competes with it for the reagent ion, i.e., lowering the sensitivity, or whether the presence of water
335 molecule offers a loosely bound third body to stabilize the adduct by removing the excess energy after the
336 {M-(reagent ion)} collision, thereby increasing sensitivity. While post measurement correction can be
337 performed, it is labor-intensive and prone to errors as each compound has essentially a unique humidity
338 dependence. To overcome this fundamental drawback, the Vocus AIM reactor introduces a system to
339 mitigate water vapor dependencies using a dopant. The dopant effectively replaces water vapor, the
340 dominant ligand in the switching reaction involving the reagent ions and the analyte molecules. A dopant
341 could in principle be any molecule that binds (forms an adduct) with the reagent ion more strongly than the
342 reagent ion and water. In this way, the dopant can displace the water molecules that would normally be
343 attached to the reagent ions with a compound that is not variable or present in significant concentrations in

344 the sample gas. The following equations show the modified reaction mechanism in the presence of a dopant
345 (D) in the case of iodide anions.



348 The modified reaction mechanism no longer significantly depends on varying water vapor conditions as
349 long as the dopant molecule is present in sufficiently high concentrations to replace most of the water
350 ligand. In the above chemical ionization mechanism for iodide anions, the challenge can be to choose a
351 suitable dopant. While the dopant must efficiently displace the water that is bound to iodide, it is also
352 desirable for the binding energy to be close to that of water. This ensures that the net chemical ionization
353 selectivity remains nearly unchanged compared to the dopant-free conditions. If a dopant with a very high
354 binding energy is selected, it will introduce a binding energy ionization threshold which will significantly
355 change the selectivity of the given ion chemistry by essentially removing all weakly bound adducts from
356 the spectra. Here we investigate three different dopants including acetonitrile, methanol, and acetone. These
357 compounds weakly interact with iodide anions and have a high vapor pressure which facilitates their easy
358 introduction into the reactor. This is typically achieved using a mass flow controller (Bronkhorst Low Delta
359 P, 30 sccm MFC) that draws from the headspace of a liquid reservoir, effectively minimizing the net dilution
360 (net sample dilution ~1%).

361 For each of the evaluated dopants, stable concentrations of formic, nitric, and acrylic acids were
362 introduced into the entrance of the reactor. The incoming air was humidified with two mass flow controllers,
363 one delivering dry nitrogen and the other passing dry nitrogen through a water bubbler held at room
364 temperature. The ratio of the two mass flow controllers was programmatically changed to simulate changes
365 in sample humidity for each dopant flow rate. Figure 3 illustrates how the systematic introduction of each
366 of these dopants at different mass flow rates influences the reactor's detection efficiency for nitric, formic,
367 and acrylic acids under changing humidity levels (0 - 100% relative humidity at 25°C). These compounds
368 were selected as characteristic compounds for the iodide adduct system, each demonstrating a distinct

369 sensitivity dependence on humidity which follows the changes in the water-iodide cluster distribution (Lee
370 et al., 2014).

371 Under dopant-free conditions, we expect nitric acid to first sharply increase from dry conditions to
372 humid conditions followed by a plateau at water vapor partial pressures of ~ 0.25 mbar. This can be
373 attributed to nitric acid's high binding enthalpy with I^- and a small, (1kcal/mol), difference to the binding
374 enthalpy to $\text{I}(\text{H}_2\text{O})^-$ that is sufficiently compensated by the kinetic stabilization from the increased number
375 of vibrational modes due to the addition of the water molecule (Lopez et al., 2016). In the case of acrylic
376 acid, the sensitivity as a function of water vapor concentration falls rapidly following the availability of
377 unhydrated iodide anions. With increasing water vapor concentrations, the weak binding energy between
378 acrylic acid is not enough to overcome the competition with water for the bare iodide ions. Formic acid is
379 between these two extremes, initially stabilized by the presence of water, but ultimately in competition with
380 water for iodide ions as the second water cluster forms reducing the sensitivity at higher absolute humidity.

381 In the doped conditions, the humidity dependencies are significantly reduced for all molecules. The
382 dopant and humidity scans demonstrate the net effect of the different dopants for each molecule as a
383 function of the total dopant flow introduced. While methanol and acetone to a certain extent shift the reagent
384 ion distribution, they are not present in high enough concentrations to fully displace the water and stabilize
385 the reagent ion distribution against changes driven by humidity changes. Acetonitrile on the other hand
386 demonstrates a significant shift in reagent ion distributions and a significant damping of the humidity
387 dependency, particularly at flows greater than ~ 20 sccm. With acetonitrile as the dopant, the change in
388 sensitivity across the humidity range is reduced to a deviation of $<20\%$ relative to dry conditions for all
389 model compounds, more for formic acid and nitric acid ($<10\%$). From the relative flattening of the humidity
390 dependence, for iodide anions (Caldwell et al., 1989) acetonitrile emerges as the most efficient dopant tested
391 reducing sensitivity variability across most analytes to a deviation that becomes negligible for ambient
392 analysis.

393 While this example focused on the dopant's presence in the reaction mechanism for iodide anions,
394 the same concept holds for any adduct forming ion including Br^- and Cl^- . For example, when generating

395 protonated ammonium ions in the presence of acetone, the formation of the $C_3H_6O-NH_4^+$ adduct with
396 acetone itself acts as a dopant and greatly suppresses the water vapor dependency, as demonstrated in Figure
397 S4. Where ammonium ions alone exhibit order of magnitude humidity dependencies when operated at
398 elevated pressure, this variability is reduced to <30% with significant acetone present as the dopant
399 (Canaval et al., 2019; Xu et al., 2022; Li et al, 2023), greatly simplifying analysis.

400 3.3 Sensitivity and Limits of Detection

401 Sensitivities for a variety of compounds were evaluated for each ion chemistry to quantify the overall
402 instrument performance. Calibrations were typically done at one or two different concentration steps in the
403 range of a few ppbv. Sensitivities were normalized to the number of recorded reagent ions measured at the
404 detector, which provides a straightforward method for correcting for any absolute fluctuations in the
405 instrument's response over time and referenced to a recorded total reagent ion current of 10^6 ions/second.
406 Typical reagent ion currents measured on the Vocus AIM reactors are between $3 - 6 \times 10^6$ ions/second for
407 iodide anions and benzene cations. Results from the calibration experiments are summarized in Table 1
408 organized by reagent ion. The compounds for calibration were specifically selected based on their
409 selectivity for each reagent ion and their relative ease of producing stable concentrations. A diverse range
410 of hydrocarbons, reactive nitrogen species, organic compounds (with various volatilities), and inorganic
411 acids can be detected with high sensitivities often greater than ~ 10 cps/ppt/ 1×10^6 RI. The sensitivity of
412 the Vocus AIM reactor does not necessarily surpass that of previous low and medium-pressure reactors
413 (Lee et al., 2014, 2018; Ye et al., 2021; Xu et al., 2022) in an absolute sense, however, the sensitivity is in
414 the same approximate range and reaches the extremely low limit of detections (LoD) ranging from 0.1 to 5
415 ppt for most compounds. LoD measurements were performed by introducing 2 slpm of dry UHP N₂ (i.e.,
416 background measurement) for 10-15 minutes. The LoD was estimated by using Tofware and calculating
417 the Allan variance (i.e., the stability of the signal over time). Finally, the LoD corresponds to 3 standard
418 deviations (sigma) of the Allen variance and is determined as a function of integration time estimation. An
419 example, using acetone dimers as reagent ions, the LoD for ammonia is about 10 ppt (1 min averaging),

420 which is 1-8 times lower than previously reported for this compound (You et al., 2014; Dong et al., 2022;
421 Schobesberger et al., 2022). Additionally, using a benzene cation as a reagent ion, the LoD for
422 monoterpenes (e.g., 0.2 ppt for α -pinene at 1 min) can even surpass conventional PTR techniques, including
423 the Vocus PTR (i.e., 4 ppt for α -pinene at 1 min; Krechmer et al., 2018) and similar to the FUSION PTR
424 (i.e., 0.1 pptv for 1 minute;).

425 The absolute sensitivity of the instrument depends fundamentally on the reaction time and collision
426 frequency (pressure) as well as the absolute number of generated reagent ions introduced into the reactor.
427 Figure 4a shows the dependence of the measured sensitivity of levoglucosan on the reactor pressure. By
428 increasing the pressure from 35 to 75 mbar the sensitivity of the instrument can be increased by a factor of
429 ~ 4 which is consistent with the increase expected based on reaction time and collision frequency. Operating
430 at higher pressures can be beneficial in pristine or highly diluted environments, where the concentrations
431 of target compounds can reside in the sub-parts-per-trillion (sub-ppt) range. A nominal operation pressure
432 of 50 mbar provides a good balance between sensitivity and linear range which under typical conditions
433 extends to ~ 100 -200 ppbv depending on the analyte (Figure 4b). This allows the standard conditions (which
434 are a compromise between sensitivity and linear range) of the Vocus AIM reactor to operate equally well
435 in pristine and polluted environments with the same configuration. In highly polluted environments where
436 the total detectable mass concentrations greatly exceed the linear range of the instrument, reagent ion
437 normalization can compensate for up to 50% of reagent ion depletion before normalization errors begin to
438 accumulate. In such conditions, the incoming sample flow would need to be diluted, to maintain
439 concentrations within the normalization range.

440 Finally, taking advantage of the improved time response and the possibility of operating more than
441 one VUV lamp on the Vocus AIM reactor (Figure 1), a fast switch between different ion chemistries at up
442 to 2 Hz is now possible as shown in Figure S5. This valuable feature allows the Vocus AIM reactor to
443 extend the variety of compounds detected by one instrument within a single polarity, as the mass analyzer
444 used in this study had polarity switching timescales of 5-10 minutes.

445

446 3.4 Vocus AIM Performance for Atmospheric Applications

447 To evaluate the bulk detection capabilities of Vocus AIM we measured oxidation products from the OH/O₃
448 initiated oxidation of α -pinene using a steady-state flow tube setup. This reaction mechanism was chosen
449 because it is a well-studied system resulting in a suite of oxidation products spanning a wide range of
450 functionalities. Additionally, it generates molecules with a wide range of molecular masses, from lightly
451 oxidized monomers to heavily oxidized dimers. In total, four AIM reagent ion chemistries, namely NH₄⁺,
452 Cl⁻, I⁻ and NO₃⁻ were used to investigate their relative detection efficiency (selectivity) towards produced
453 OVOCs. AIM offers an ideal method for evaluating ion chemistries as it ensures uniformity in the
454 introduction of all reagent ions and utilizes the same analytical instrument for comparison. This approach
455 effectively eliminates the instrument-to-instrument variability, thus providing a highly direct and unbiased
456 comparison of ion chemistry and detection efficacy for a variety of mixed organic compounds.

457 **RO₂ radicals generated from the combined ozonolysis and OH radical reaction of α -pinene can**
458 **further react yielding mixed oxidation products during the reaction time in the flow tube.** Among the
459 different RO₂ radicals formed, C₁₀H₁₅O_{>3} and C₁₀H₁₇O_{>2} were detected by the different reagent ions used.
460 While the mass spectra are generally similar between the different reagent ion chemistries, there are some
461 notable differences in the detection efficiencies. NO₃⁻ ion-based chemistry is by far the most selective of
462 the reagent ions tested. A smaller group of compounds was detected, with a particular inclination towards
463 the most heavily oxidized monomers and gas-phase dimer species. The variable selectivity of the different
464 ion chemistries is demonstrated in Figure 5, organized by the increase of reagent ion selectivity. NH₄⁺ and
465 Cl⁻ are the least selective ions evaluated, highlighted by the large ion signal intensity of compounds m/Q <
466 100 Th (least oxidized) and the largest number of absolute compounds detected. While the sensitivity
467 towards less oxidized compounds is limited to the less selective reagent ions (i.e., NH₄⁺ and Cl⁻), more
468 selective reagent ions excel at detecting the lower concentration of more oxidized compounds. The
469 selectivity of the reagent ion plays a pivotal role in limiting the backgrounds and potential isobaric
470 interferences that might hamper the detection of the compounds of interest. With the AIM reactor and the
471 right selection of reagent ion, even the highest oxidized RO₂ radicals (e.g., C₁₀H₁₇O₇ and C₁₀H₁₅O₈), and

472 dimeric products (e.g., C₁₉H_{28,30}O_x C₂₀H_{30,32}O_x) can be identified under relevant atmospheric conditions,
473 highlighting the very high sensitivity and versatility of the Vocus AIM reactor.

474 To demonstrate the bulk detection properties of the different reagent ion chemistries more clearly,
475 we categorized each compound according to its estimated volatility. Due to the lack of authentic standards
476 measuring the vapor pressure of oxygenated organic molecules (OOMs) remains an analytical challenge.
477 To overcome this problem, model calculations have been developed to estimate the vapor pressure using,
478 for example, structure-based estimations and formula-based estimations. The volatility basis set (VBS)
479 framework has been established by Donahue et al. (2011) and is widely used in atmospheric chemistry to
480 estimate the volatility of products measured by mass spectrometry techniques. The VBS parameterization
481 is useful for classifying the wide range of OOMs into multiple volatility groups, including extremely low
482 volatility organic compounds (ELVOC) and low volatility organic compounds (LVOC) based on their
483 effective saturation concentration (C*) in the unit of μg m⁻³. In this work, we apply the VBS
484 parameterization optimized by Li et al. (2016),

$$\log_{10}C^*(298K) = (n_C^0 - n_C)b_C - n_O b_O - 2 \frac{n_C n_O}{(n_C + n_O)} b_{CO} - n_N b_N - n_S b_S \quad (10)$$

485
486 where n_C, n_O, n_N, and n_S are the number of carbon, oxygen, nitrogen, and sulfur atoms of the specific
487 molecule, separately; n_C⁰ is the reference carbon number; b_C, b_O, b_N, and b_S are the contribution of each
488 atom to log₁₀C*, respectively; b_{CO} is the carbon-oxygen nonideality. The b coefficient values can be found
489 in Li et al. (2016). In this study, all oxidation products generated from the OH/O₃ initiated oxidation were
490 grouped into six volatility regimes; ultralow-volatility (ULVOCs, C* < 10^{-8.5} μg m⁻³), extremely low
491 volatility (ELVOCs, 10^{-8.5} < C* < 10^{-4.5} μg m⁻³), low-volatility (LVOCs, 10^{-4.5} < C* < 10^{-0.5} μg m⁻³), semi-
492 volatile (SVOCs, 10^{-0.5} < C* < 10^{2.5} μg m⁻³), intermediate-volatility organic compounds (IVOC, 10^{2.5} < C*
493 < 10^{6.5} μg m⁻³), and VOC (10^{6.5} < C* μg m⁻³) based on VBS.

494 Figure 6 illustrates the measured range of oxidation products generated by the hydroxyl radical and
495 ozone reaction with α -pinene. These products were analyzed using one mass spectrometer with AIM reactor
496 setup employing various ionization chemistries. Therefore, unlike other studies (Riva et al., 2019, Li et al.,
497 2023) this study utilizes a single instrument, thereby reducing uncertainties associated with the calibration
498 and settings of different instruments as well as the conditions during sample collection. The total signal in
499 each volatility bin represents the sum of the signal intensity of OOMs within the volatility range. Organic
500 compounds with C^* of $< 10^{-1} \mu\text{g m}^{-3}$ made up the largest signal contributions for the Vocus AIM using
501 NO_3^- -ion based chemistry (Table S2). This observation is consistent with the conventional atmospheric
502 pressure using NO_3^- as the reagent ion and indicates that the design of the Vocus AIM reactor allows the
503 detection of ELVOC and ULVOC (Riva et al., 2019; Zhang W. et al., 2023; Zhang Y. et al., 2023). This is
504 a substantial improvement for the atmospheric science community as measurement of such species is solely
505 possible with the use of atmospheric pressure interfaces which can be associated with sensitivity
506 fluctuations (e.g., RH effect). As demonstrated previously (Riva et al., 2019), I^- -ion based chemistry detects
507 oxygenated compounds with C^* ranging from 10^{-5} to $10^5 \mu\text{g m}^{-3}$ which corresponds to OOMs and start
508 being less sensitive to oxygenated compounds having fewer oxygen atoms and are included in the IVOC
509 fraction. While Cl^- and NH_4^+ can also measure OOM with C^* as low as $10^{-5} \mu\text{g m}^{-3}$ the weak selectivity of
510 these ion-based chemistries allows them to measure a wider range of compounds (i.e., IVOCs and VOCs).
511 IVOCs and VOCs generally include less oxygenated VOCs with shorter carbon skeletons and comprise the
512 main fraction of organics formed from the oxidation of pinene (Isaacman-VanWertz et al., 2018). We stress
513 here that while it was not possible to detect ULVOC and ELVOC using I^- , Cl^- , NH_4^+ -ion based chemistries
514 it is purely a selectivity limitation of the more general reagent ions not of absolute sensitivity as all the
515 tested reagent ions have similar overall absolute sensitivities. Nitrate reagent ions benefit from the high
516 selectivity, which also manifests in a lower background signal therefore enabling nitrate anion chemistry to
517 detect ULVOC and ELVOC. With the significantly lower background concentrations of nitrate ions, the
518 detection of compounds at extremely low concentrations (as low as 10-100 ppqv) becomes possible.

519 Differences in the contribution of these compound groups (i.e., relative signal contribution to total
520 OOMs) with previous work could be due to different sensitivities of the instruments towards organic
521 compounds with varying oxidation extents (Riva et al., 2019). In addition, experimental conditions (e.g.,
522 RH, temperature, precursor concentration) and setup (flow tube reactor, atmospheric simulation chambers)
523 can greatly impact the distribution of OOMs retrieved by MS techniques. By carefully selecting the type of
524 reagent ion, the combined volatility distribution can cover from VOCs to OOMs, with varying O:C ratios
525 and volatility ranges (Figure 6) all within a single instrument. The Vocus AIM can therefore provide a more
526 complete picture of the volatility distribution of gaseous organic and inorganic compounds found in the
527 atmosphere.

528 Conclusions

529 The primary goal of this work was to evaluate the performance of the newly designed Vocus AIM reactor
530 to determine the time response, sensitivity, and selectivity using multiple reagent ions. Of specific
531 importance, we introduced and demonstrated the utility of a dopant-based water vapor suppression system
532 which improves data quality and reduces the number of corrections required during analysis. By comparing
533 detection efficiency for different compounds, we demonstrated that the Vocus AIM captures nearly the
534 entire range of OVOC, spanning from VOC to ULVOC by using different types of reagent ions. Through
535 the optimization of reactor geometry and materials, the time response of the Vocus AIM reactor is greatly
536 improved even for sticky and reactive compounds. The high sensitivity achieves sub-ppt detection limits
537 for a range of VOCs and VICs. The innovative design of the new reactor substantially eliminated this
538 humidity sensitivity, facilitating more straightforward measurements of samples with water vapor and
539 simplifying data interpretation. This improvement is crucial for robust and reliable analysis across a
540 spectrum of environmental samples. As a result, the Vocus AIM reactor represents a highly versatile
541 platform able to measure the wide variety of VOCs and VICs in the atmosphere using a single instrument.
542

543 **Conflicts of interest**

544 All (co-)authors, except S.P. and J.A.T. work for ToFWerk AG, which is commercializing the
545 Vocus-AIM mass spectrometer.

546 **Author Contributions**

547 M.R., V.P., F.L., conceive the study. M.R., V.P., C.F., P.B., S.P., S.J., and F.L. collected and
548 analyzed the data. P.S., U.R., and F.L. conceived the design of the Vocus AIM reactor. M.R., V.P.,
549 F.L. wrote the manuscript. All authors discussed the results and commented on the paper.

550

551 **Acknowledgements:**

552 We would also like to thank Withtech Inc, and Minji Park for providing calibration comparison
553 data with the Picarro CRDS.

554

555 **References**

- 556 Berndt, T., Richters, S., Kaethner, R., Voigtlander, J., Stratmann, F., Sipila, M., Kulmala, M., and
557 Herrmann, H.: Gas-Phase Ozonolysis of Cycloalkenes: Formation of Highly Oxidized RO₂ Radicals and
558 Their Reactions with NO, NO₂, SO₂, and Other RO₂ Radicals, *J. Phys. Chem. A*, 119, 10336-10348,
559 10.1021/acs.jpca.5b07295, 2015.
- 560 Berndt, T., Herrmann, H., and Kurten, T.: Direct Probing of Criegee Intermediates from Gas-Phase
561 Ozonolysis Using Chemical Ionization Mass Spectrometry, *J. Am. Chem. Soc.*, 139, 13387-13392,
562 10.1021/jacs.7b05849, 2017.
- 563 Berndt, T., Mentler, B., Scholz, W., Fischer, L., Herrmann, H., Kulmala, M., and Hansel, A.: Accretion
564 Product Formation from Ozonolysis and OH Radical Reaction of alpha-Pinene: Mechanistic Insight and
565 the Influence of Isoprene and Ethylene, *Environ. Sci. Technol.*, 52, 11069-11077,
566 10.1021/acs.est.8b02210, 2018.
- 567 Bertram, T. H., Kimmel, J. R., Crisp, T. A., Ryder, O. S., Yatavelli, R. L. N., Thornton, J. A., Cubison, M.
568 J., Gonin, M. and Worsnop, D. R.: A field-deployable, chemical ionization time-of-flight mass
569 spectrometer, *Atmos. Meas. Tech.*, 4(7), 1471–1479, doi:10.5194/amt-4-1471-2011, 2011.
- 570 Bianchi, F., Kurten, T., Riva, M., Mohr, C., Rissanen, M. P., Roldin, P., Berndt, T., Crounse, J. D.,
571 Wennberg, P. O., Mentel, T. F., Wildt, J., Junninen, H., Jokinen, T., Kulmala, M., Worsnop, D. R.,
572 Thornton, J. A., Donahue, N., Kjaergaard, H. G., and Ehn, M.: Highly Oxygenated Organic Molecules
573 (HOM) from Gas-Phase Autoxidation Involving Peroxy Radicals: A Key Contributor to Atmospheric
574 Aerosol, *Chem. Rev.*, 119, 3472-3509, 10.1021/acs.chemrev.8b00395, 2019.
- 575 Breitenlechner, M., Fischer, L., Hainer, M., Heinritzi, M., Curtius, J., and Hansel, A.: PTR3: An Instrument
576 for Studying the Lifecycle of Reactive Organic Carbon in the Atmosphere, *Anal. Chem.*, 89, 5824-5831,
577 10.1021/acs.analchem.6b05110, 2017.

578 Breitenlechner, M., Novak, G. A., Neuman, J. A., Rollins, A. W., and Veres, P. R.: A versatile vacuum
579 ultraviolet ion source for reduced pressure bipolar chemical ionization mass spectrometry, *Atmos. Meas.*
580 *Tech.*, 15, 1159–1169, <https://doi.org/10.5194/amt-15-1159-2022>, 2022.

581 Bruderer, T., Gaisl, T., Gaugg, M.T., Nowak, N., Streckenbach, B., Müller, S., Moeller, A., Kohler, M.,
582 and Zenobi, R.: On-Line Analysis of Exhaled Breath, *Chem. Rev.*, 119, 19, 10803–10828,
583 10.1021/acs.chemrev.9b00005, 2019.

584 Caldwell, G. W., Masucci, J. A., and Ikonou, M. G.: Negative ion chemical ionization mass
585 spectrometry—binding of molecules to bromide and iodide anions, *Organic Mass Spectrometry*, 24, 8–
586 14, 10.1002/oms.1210240103, 1989.

587 Canaval, E., Hyttinen, N., Schmidbauer, B., Fischer, L., and Hansel, A.: NH_4^+ Association and Proton
588 Transfer Reactions With a Series of Organic Molecules, *Front. Chem.*, 7, 10.3389/fchem.2019.00191,
589 2019.

590 Crouse, J. D., Nielsen, L. B., Jørgensen, S., Kjaergaard, H. G., and Wennberg, P. O.: Autoxidation of
591 Organic Compounds in the Atmosphere, *J. Phys. Chem. Lett.*, 4, 3513–3520, 10.1021/jz4019207, 2013.

592 Donahue, N. M., Epstein, S. A., Pandis, S. N., and Robinson, A. L.: A two-dimensional volatility basis set:
593 1. organic-aerosol mixing thermodynamics, *Atmos. Chem. Phys.*, 11, 3303–3318, 10.5194/acp-11-3303-
594 2011, 2011.

595 Dong, F., Li, H., Liu, B., Liu, R., and Hou K.: Protonated acetone ion chemical ionization time-of-flight
596 mass spectrometry for real-time measurement of atmospheric ammonia, *J. Environ. Sci.*, 14, 66–74,
597 10.1016/j.jes.2021.07.023, 2022.

598 Ehn, M., Thornton, J. A., Kleist, E., Sipila, M., Junninen, H., Pullinen, I., Springer, M., Rubach, F.,
599 Tillmann, R., Lee, B., Lopez-Hilfiker, F., Andres, S., Acir, I. H., Rissanen, M., Jokinen, T.,
600 Schobesberger, S., Kangasluoma, J., Kontkanen, J., Nieminen, T., Kurten, T., Nielsen, L. B., Jørgensen,
601 S., Kjaergaard, H. G., Canagaratna, M., Maso, M. D., Berndt, T., Petaja, T., Wahner, A., Kerminen, V.
602 M., Kulmala, M., Worsnop, D. R., Wildt, J., and Mentel, T. F.: A large source of low-volatility secondary
603 organic aerosol, *Nature*, 506, 476–479, 10.1038/nature13032, 2014.

604 Eisele, F.L., Tanner, D.J., Measurement of the gas phase concentration of H_2SO_4 and methane sulfonic
605 acid and estimates of H_2SO_4 production and loss in the atmosphere, *J. Geophys. Res. Atmo.*, 98, 9001-
606 9010, 10.1029/93JD00031, 1993.

607 Hallquist, M., Wenger, J. C., Baltensperger, U., Rudich, Y., Simpson, D., Claeys, M., Dommen, J.,
608 Donahue, N. M., George, C., Goldstein, A. H., Hamilton, J. F., Herrmann, H., Hoffmann, T., Iinuma,
609 Y., Jang, M., Jenkin, M. E., Jimenez, J. L., Kiendler-Scharr, A., Maenhaut, W., McFiggans, G., Mentel,
610 T. F., Monod, A., Prévôt, A. S. H., Seinfeld, J. H., Surratt, J. D., Szmigielski, R., and Wildt, J.: The
611 formation, properties and impact of secondary organic aerosol: current and emerging issues, *Atmos.*
612 *Chem. Phys.*, 9, 5155–5236, 10.5194/acp-9-5155-2009, 2009.

613 Hansel, A., Scholz, W., Mentler, B., Fischer, L., and Berndt, T.: Detection of RO_2 radicals and other
614 products from cyclohexene ozonolysis with NH_4^+ and acetate chemical ionization mass spectrometry,
615 *Atmo. Environ.*, 186, 248–255, 10.1016/j.atmosenv.2018.04.023, 2018.

616 Isaacman-VanWertz, G. and Aumont, B.: Impact of organic molecular structure on the estimation of
617 atmospherically relevant physicochemical parameters, *Atmos. Chem. Phys.*, 21, 6541–6563,
618 10.5194/acp-21-6541-2021, 2021.

619 Ji, Y., Huey, L. G., Tanner, D. J., Lee, Y. R., Veres, P. R., Neuman, J. A., Wang, Y., and Wang, X.: A
620 vacuum ultraviolet ion source (VUV-IS) for iodide–chemical ionization mass spectrometry: a substitute
621 for radioactive ion sources, *Atmos. Meas. Tech.*, 13, 3683–3696, 10.5194/amt-13-3683-2020, 2020.

622 Krechmer, J., Lopez-Hilfiker, F., Koss, A., Hutterli, M., Stoermer, C., Deming, B., Kimmel, J., Warneke,
623 C., Holzinger, R., Jayne, J. T., Worsnop, D. R., Fuhrer, K., Gonin, M. and de Gouw, J. A.: Evaluation
624 of a New Reagent-Ion Source and Focusing Ion-Molecule Reactor for use in Proton-Transfer-Reaction
625 Mass Spectrometry, *Anal. Chem.*, 10.1021/acs.analchem.8b02641, 2018.

626 Lavi, A., Vermeuel, M. P., Novak, G. A., and Bertram, T. H.: The sensitivity of benzene cluster cation
627 chemical ionization mass spectrometry to select biogenic terpenes, *Atmos. Meas. Tech.*, 11, 3251–3262,
628 <https://doi.org/10.5194/amt-11-3251-2018>, 2018.

629 Lee, B. H., Lopez-Hilfiker, F. D., Mohr, C., Kurten, T., Worsnop, D. R., and Thornton, J. A.: An iodide-
630 adduct high-resolution time-of-flight chemical-ionization mass spectrometer: application to atmospheric
631 inorganic and organic compounds, *Environ. Sci. Technol.*, 48, 6309-6317, 10.1021/es500362a, 2014.

632 Lee, B. H., Lopez-Hilfiker, F. D., Veres, P.R., McDuffie, E.E., Fibiger, D.L., Sparks, T.M., Ebben, C.J.,
633 Green, J.R., Schroder, J.C., Campuzano-Jost, P., Iyer, S., D'Ambro, E.A., Schobesberger, S., Brown,
634 S.S., Wooldridge, P.J., Cohen, R.C., Fiddler, M.N., Bililign, S., Jimenez, J.L., Kurtén, T., Weinheimer,
635 A.J., Jaegle, L., and Thornton, J. A.: Flight Deployment of a High-Resolution Time-of-Flight Chemical
636 Ionization Mass Spectrometer: Observations of Reactive Halogen and Nitrogen Oxide Species, *J.*
637 *Geophys Res. Atmos.*, 123, 7670-7686, 10.1029/2017JD028082, 2018.

638 Li, Y., Pöschl, U., and Shiraiwa, M.: Molecular corridors and parameterizations of volatility in the chemical
639 evolution of organic aerosols, *Atmos. Chem. Phys.*, 16, 3327-3344, 10.5194/acp-16-3327-2016, 2016.

640 Li, D., Wang, D., Caudillo, L., Scholz, W., Wang, M., Tomaz, S., Marie, G., Surdu, M., Eccli, E., Gong,
641 X., Gonzalez-Carracedo, L., Granzin, M., Pfeifer, J., Rörup, B., Schulze, B., Rantala, P., Perrier, S.,
642 Hansel, A., Curtius, J., Kirkby, J., Donahue, N. M., George, C., El-Haddad, I., and Riva, M.: Ammonium
643 CI-Orbitrap: a tool for characterizing the reactivity of oxygenated organic molecules, *Atmos. Meas.*
644 *Tech. Discuss.* [preprint], <https://doi.org/10.5194/amt-2023-149>, in review, 2023.

645 Lopez-Hilfiker, F. D., Iyer, S., Mohr, C., Lee, B. H., D'Ambro, E. L., Kurtén, T. and Thornton, J.
646 A.: Constraining the sensitivity of iodide adduct chemical ionization mass spectrometry to
647 multifunctional organic molecules using the collision limit and thermodynamic stability of iodide ion
648 adducts, *Atmos. Meas. Tech.*, 9(4), 1505–1512, doi:10.5194/amt-9-1505-2016, 2016.

649 Mazzucotelli, M., Farneti, B., Khomenko, I., Gonzalez-Estanol, K., Pedrotti, M., Fragasso, M., Capozzi,
650 V., and Biasioli, F.; *Green Analytical Chemistry*, 3, 10.1016/j.greeac.2022.100041, 2022.

651 Morris, M. A., Pagonis, D., Day, D. A., de Gouw, J. A., Ziemann, P. J., and Jimenez, J. L.: Absorption of
652 VOCs by polymer tubing: implications for indoor air and use as a simple gas-phase volatility separation
653 technique, *EGUsphere* [preprint], <https://doi.org/10.5194/egusphere-2023-1241>, 2023.

654 Palm, B.P., Liu, X., Jimenez, X.L., and Thornton, J. A.: Performance of a new coaxial ion–molecule
655 reaction region for low-pressure chemical ionization mass spectrometry with reduced instrument wall
656 interactions, *Atmos. Meas. Tech.*, 12, 5829–5844, doi.org/10.5194/amt-12-5829-2019, 2019

657 Pfeifer, J., Simon, M., Heinritzi, M., Piel, F., Weitz, L., Wang, D., Granzin, M., Müller, T., Bräkling, S.,
658 Kirkby, J., Curtius, J., and Kürten, A.: Measurement of ammonia, amines and iodine compounds using
659 protonated water cluster chemical ionization mass spectrometry, *Atmos. Meas. Tech.*, 13, 2501–2522,
660 <https://doi.org/10.5194/amt-13-2501-2020>, 2020.

661 Reinecke, T., Leiminger, M., Jordan, A., Wisthaler, A., and Müller, M.: Ultrahigh Sensitivity PTR-MS
662 Instrument with a Well-Defined Ion Chemistry, *Anal. Chem.*, 95, 11879–11884,
663 <https://doi.org/10.1021/acs.analchem.3c02669>, 2023.

664 Rissanen, M. P., Mikkilä, J., Iyer, S., and Hakala, J.: Multi-scheme chemical ionization inlet (MION) for
665 fast switching of reagent ion chemistry in atmospheric pressure chemical ionization mass spectrometry
666 (CIMS) applications, *Atmos. Meas. Tech.*, 12, 6635-6646, 10.5194/amt-12-6635-2019, 2019.

667 Riva, M., Rantala, P., Krechmer, J. E., Peräkylä, O., Zhang, Y., Heikkinen, L., Garmash, O., Yan, C.,
668 Kulmala, M., Worsnop, D., and Ehn, M.: Evaluating the performance of five different chemical
669 ionization techniques for detecting gaseous oxygenated organic species, *Atmos. Meas. Tech.*, 12, 2403-
670 2421, 10.5194/amt-12-2403-2019, 2019.

671 Schobesberger, S., D'Ambro, E. L., Vettikkat, L., Lee, B. H., Peng, Q., Bell, D. M., Shilling, J. E.,
672 Shrivastava, M., Pekour, M., Fast, J., and Thornton, J. A.: Airborne flux measurements of ammonia over
673 the southern Great Plains using chemical ionization mass spectrometry, *Atmos. Meas. Tech.*, 16, 247–
674 271, <https://doi.org/10.5194/amt-16-247-2023>, 2023.

675 Tang, J., Schurgers, G., and Rinnan, R.; *Process Understanding of Soil BVOC Fluxes in Natural*
676 *Ecosystems: A Review*, *Rev. Geophys.*, 57, 966-986, 10.1029/2018RG000634, 2019.

677 Vasquez, K. T., Allen, H. M., Crounse, J. D., Praske, E., Xu, L., Noelscher, A. C., and Wennberg, P. O.:
678 Low-pressure gas chromatography with chemical ionization mass spectrometry for quantification of

679 multifunctional organic compounds in the atmosphere, *Atmos. Meas. Tech.*, 11, 6815–6832,
680 <https://doi.org/10.5194/amt-11-6815-2018>, 2018.

681 Xu, L., Coggon, M. M., Stockwell, C. E., Gilman, J. B., Robinson, M. A., Breitenlechner, M., Lamplugh,
682 A., Crouse, J. D., Wennberg, P. O., Neuman, J. A., Novak, G. A., Veres, P. R., Brown, S. S., and
683 Warneke, C.: Chemical ionization mass spectrometry utilizing ammonium ions (NH₄⁺ CIMS) for
684 measurements of organic compounds in the atmosphere, *Atmos. Meas. Tech.*, 15, 7353–7373,
685 <https://doi.org/10.5194/amt-15-7353-2022>, 2022.

686 Ye, C., Yuan, B., Lin, Y., Wang, Z., Hu, W., Li, T., Chen, W., Wu, C., Wang, C., Huang, S., Qi, J., Wang,
687 B., Wang, C., Song, W., Wang, X., Zheng, E., Krechmer, J.E., Ye, P., Zhang, Z., Wang, X., Worsnop,
688 D.R., and Shao, M.: Chemical characterization of oxygenated organic compounds in the gas phase and
689 particle phase using iodide CIMS with FIGAERO in urban air, *Atmos. Chem. Phys.*, 21, 8455–8478,
690 <https://doi.org/10.5194/acp-21-8455-2021>, 2021.

691 Yuan, B., Koss, A. R., Warneke, C., Coggon, M., Sekimoto, K., and de Gouw, J. A.: Proton-Transfer-
692 Reaction Mass Spectrometry: Applications in Atmospheric Sciences, *Chem. Rev.*, 117, 13187-13229,
693 [10.1021/acs.chemrev.7b00325](https://doi.org/10.1021/acs.chemrev.7b00325), 2017.

694 You, Y., Kanawade, V. P., de Gouw, J. A., Guenther, A. B., Madronich, S., Sierra-Hernández, M. R.,
695 Lawler, M., Smith, J. N., Takahama, S., Ruggeri, G., Koss, A., Olson, K., Baumann, K., Weber, R. J.,
696 Nenes, A., Guo, H., Edgerton, E. S., Porcelli, L., Brune, W. H., Goldstein, A. H., and Lee, S. H.:
697 Atmospheric amines and ammonia measured with a chemical ionization mass spectrometer (CIMS),
698 *Atmos. Chem. Phys.*, 14, 12181-12194, [10.5194/acp-14-12181-2014](https://doi.org/10.5194/acp-14-12181-2014), 2014.

699 Zhang, W., Xu, L., Zhang, H.: Recent advances in mass spectrometry techniques for atmospheric chemistry
700 research on molecular-level, *Mass Spectrom. Rev.*, 21857, [10.1002/mas.21857](https://doi.org/10.1002/mas.21857), 2023.

701 Zhang, Y., Liu, R., Yang, D., Guo, Y., Li, M., and Hou, K.: Chemical ionization mass spectrometry:
702 Developments and applications for on-line characterization of atmospheric aerosols and trace gases,
703 *Trends Anal. Chem.*, 168, [10.1016/j.trac.2023.117353](https://doi.org/10.1016/j.trac.2023.117353), 2023.

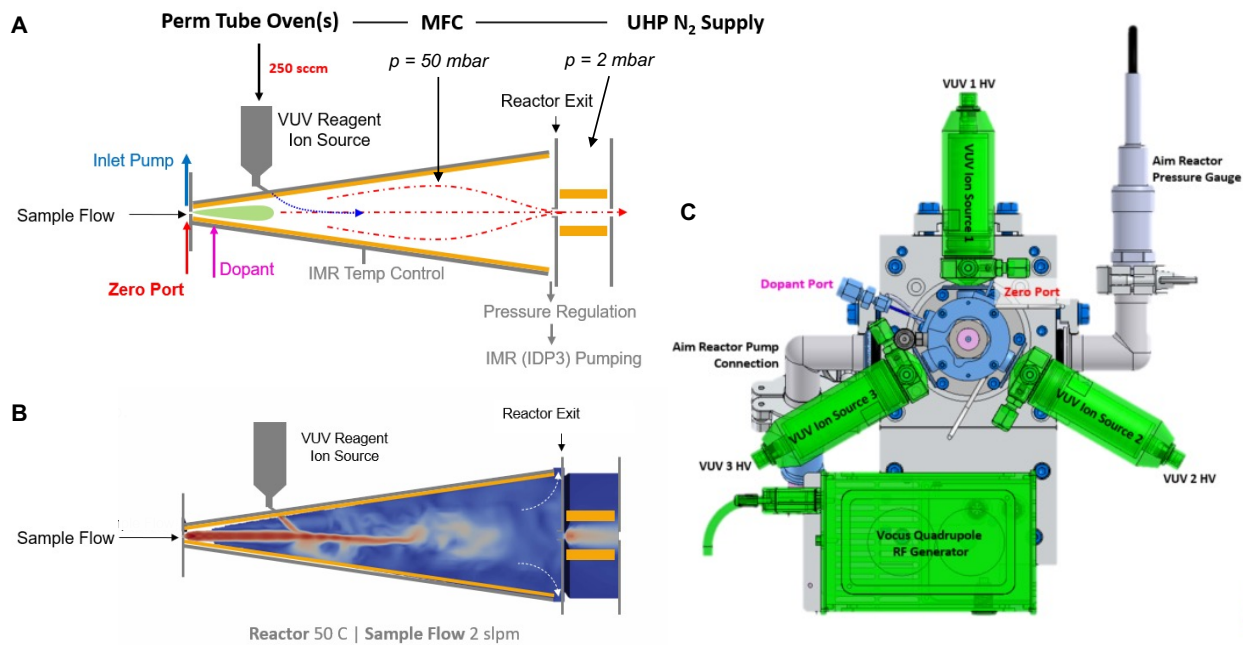
704

705 **Table 1.** Sensitivities (cps pptv⁻¹) normalized by 10⁶ detected reagent ions for different ion
 706 chemistry used with the Vocus AIM reactor.
 707

Compounds	Reagent Ion	Sensitivity (cps/ppt/ 10 ⁶ ions/s)	LoD (1-min)
toluene	Benzene (+)	7.8	0.4
m-xylene	Benzene (+)	7.6	0.2
1,2,4-trimethyl benzene	Benzene (+)	7.5	0.2
α-pinene	Benzene (+)	6.8	1.4
methyl ethyl ketone	Acetone-Ammonia (+)	5.0	4.8
ammonia	Acetone dimer (+)	1.5	1
methyl amine	Acetone dimer (+)	1.2	10
ethyl amine	Acetone dimer (+)	1.6	1
dimethyl amine	Acetone dimer (+)	2.2	1
diethyl amine	Acetone dimer (+)	2.6	1
trimethyl amine	Acetone dimer (+)	2.5	4
triethyl amine	Acetone dimer (+)	5.0	2
formic acid	Iodide (-)	2.0	0.8
levoglucosan	Iodide (-)	6.0	0.1
chlorine	Iodide (-)	5.5	3
nitric acid	Iodide (-)	4.3	5
fluoric acid	Iodide (-)	3	10
iodine	Bromide (-)	3	2

708

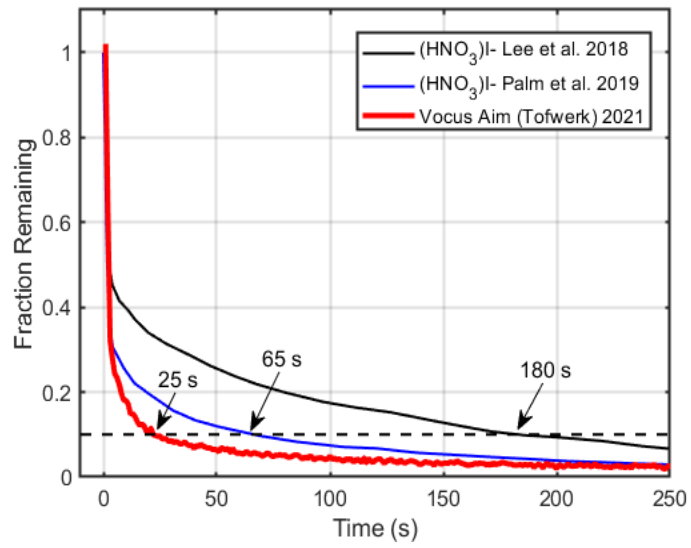
709



710

711 **Figure 1.** (A) Diagram of the Vocus AIM reactor showing the conical design and relative locations of the
 712 sample and reagent ion addition. (B) Cross-sectional view of modeled flow velocities in the AIM-IMR,
 713 showing optimized intersection of the reagent ion and sample stream flows, and limited contact of the
 714 sample gas with surfaces. (C) Key components of the Vocus AIM reactor.

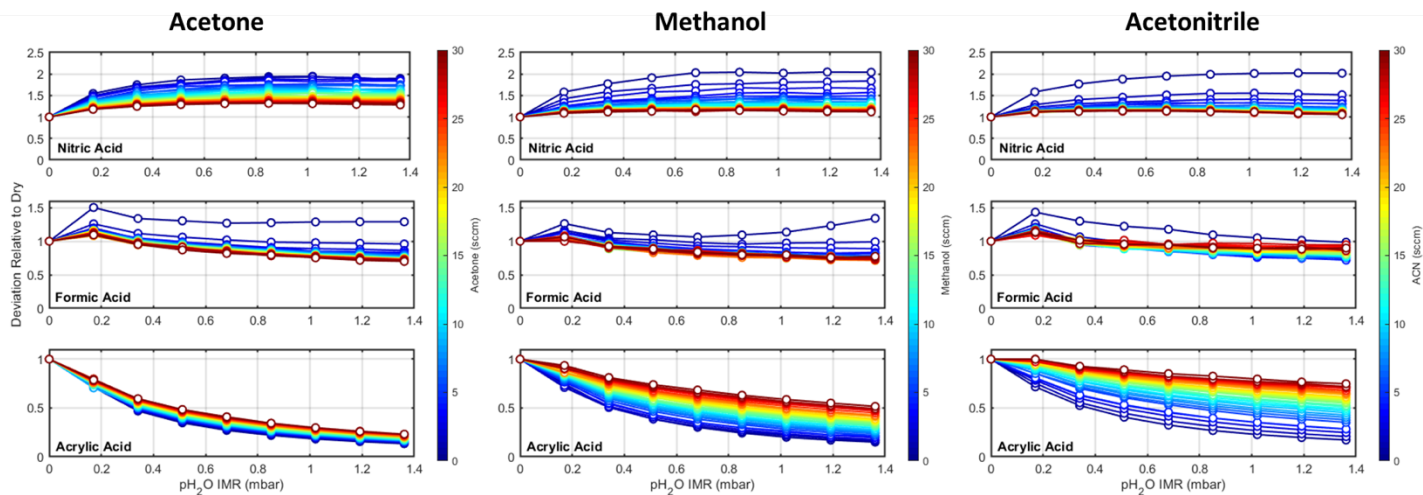
715



716

717 **Figure 2.** Time response to nitric acid of the Vocus AIM IMR compared to the previous IMR designs

718 found in the literature.



719

720 **Figure 3.** Impact of the relative humidity on the sensitivity of nitric acid, formic acid, and acrylic acid as a

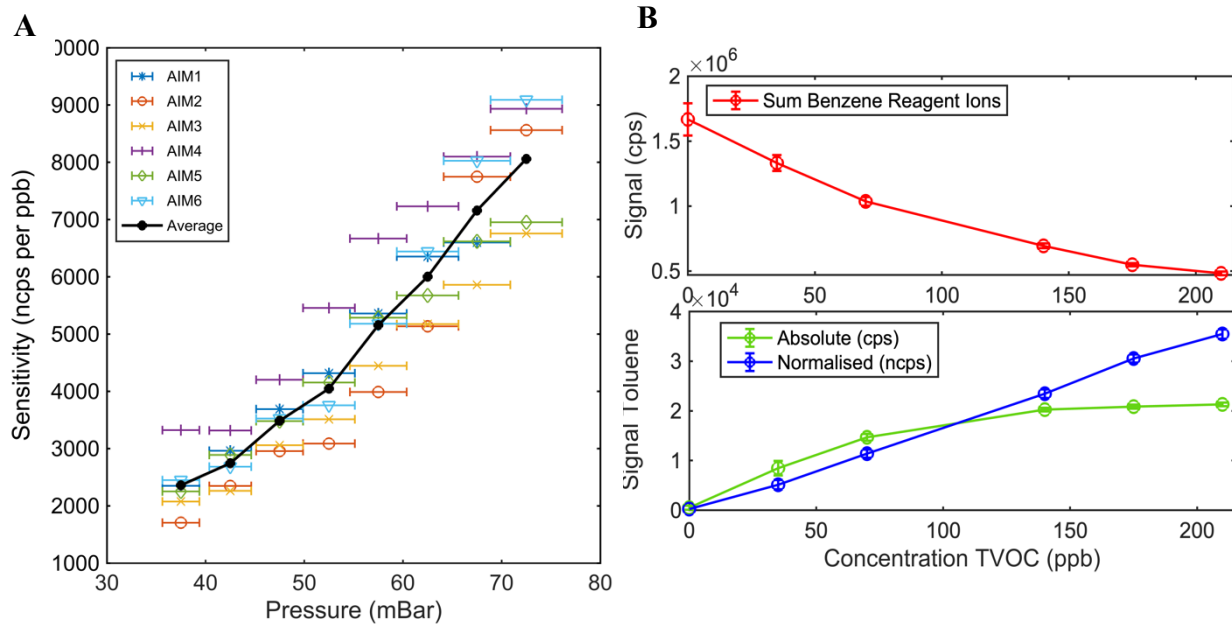
721 function of different dopant concentrations (dopants: acetone, methanol, and acetonitrile). The x-axis

722 displays the partial pressure of water, corresponding to higher humidity levels within the reactor (0-100%

723 humidity). The color gradient indicates the increasing flow of specific dopants.

724

725

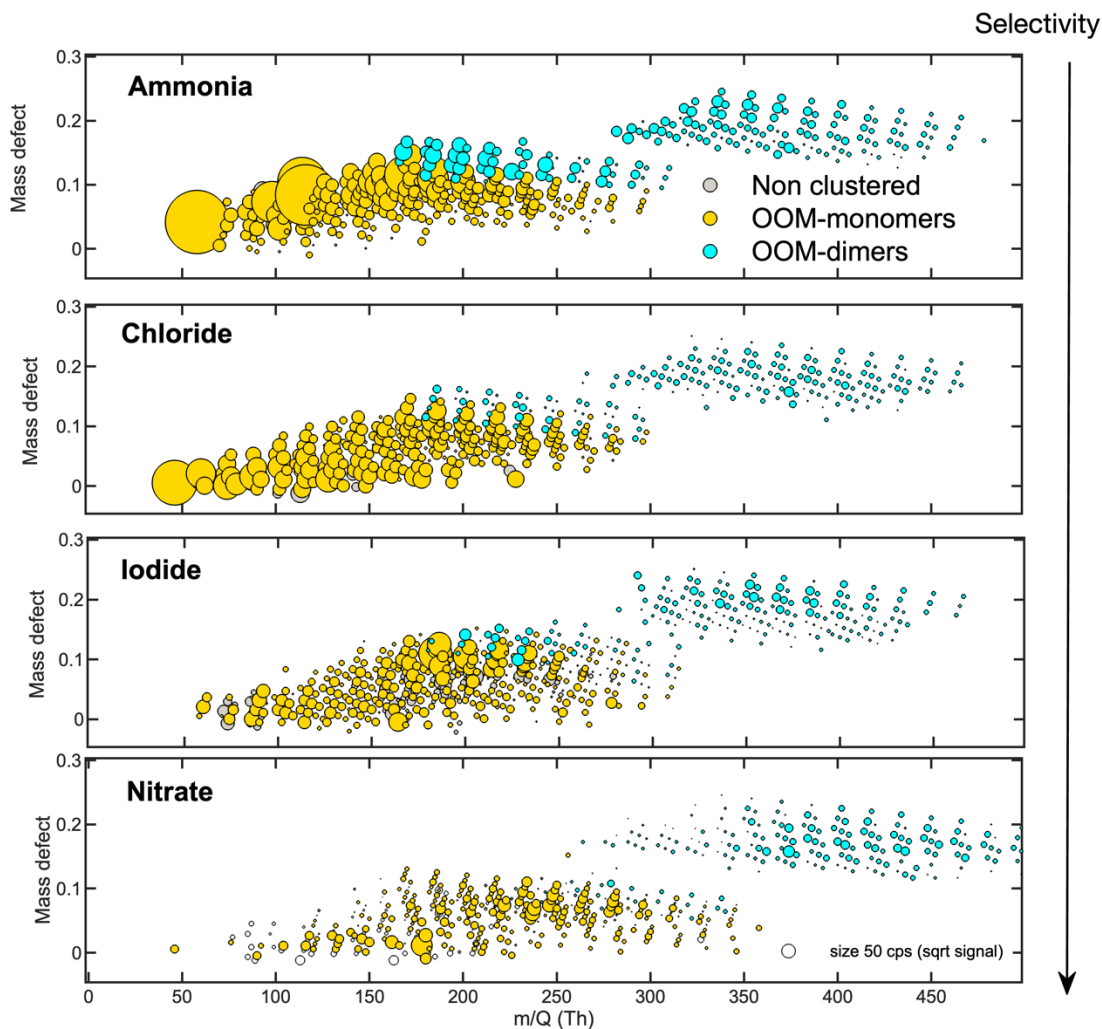


734

735 **Figure 4.** (A) presents the sensitivity dependence on the IMR pressure. The solid line represents the average
 736 sensitivity from six distinct Vocus AIM instruments, each normalized to one million reagent ions.
 737 Individual sensitivity measurements for each reactor are depicted as unique symbols. The error bars provide
 738 an estimate of the pressure gauge measurement uncertainty within 5 % of error. (B) shows the evolution of
 739 the sum of the reagent ions for Benzene cation chemistry and lower panel the ion signal intensity of toluene
 740 with and without normalization to reagent ions under a wide range of concentrations.

741

742



743 **Figure 5.** Mass defect plots of organic compounds measured by the Vocus AIM reactor using Ammonia,
 744 Chloride, Iodide, and Nitrate ion chemistries generated via the O_3/OH initiated oxidation of α -pinene. The
 745 x-axis represents the mass-to-charge ratio of the neutral analyte, the y-axis represents the corresponding
 746 mass defect, which is the difference between their exact mass and nominal mass, and the size of the circle
 747 represents the square root of the signal intensity measured for each ion.

748

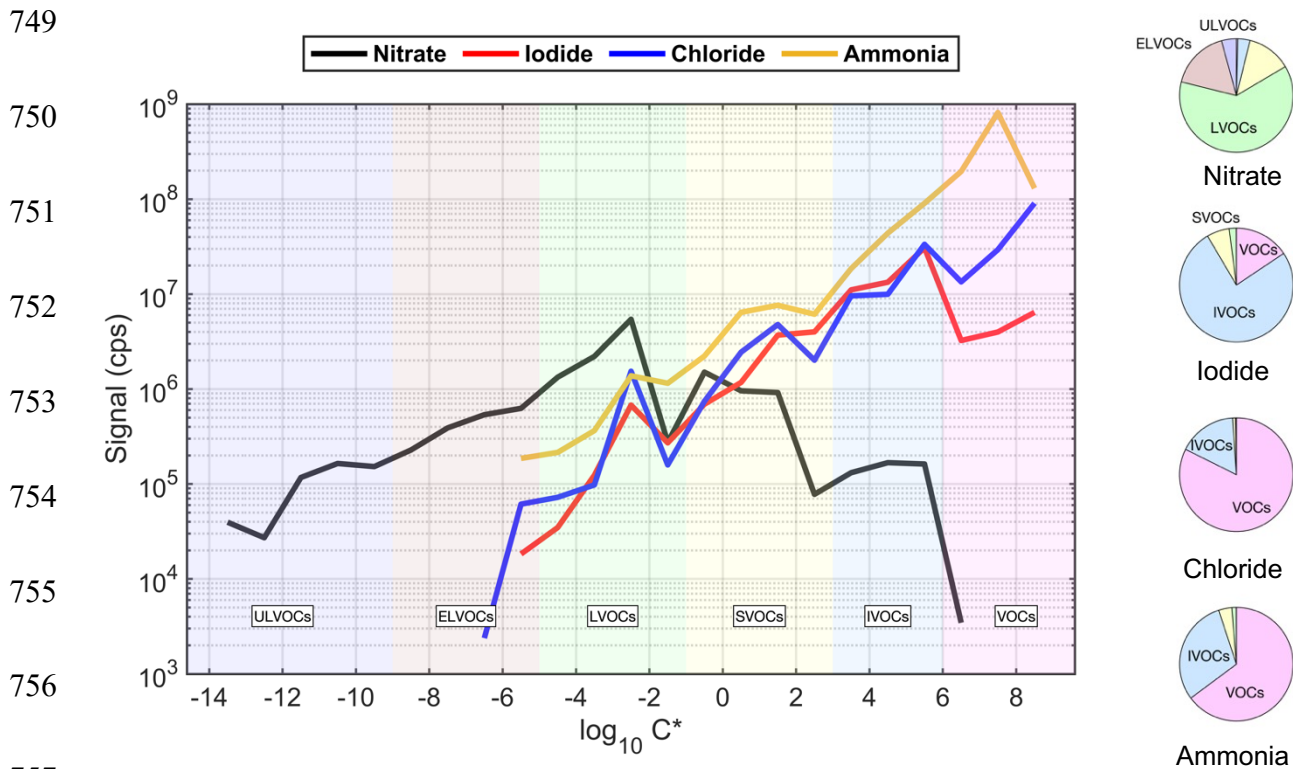


Figure 6. Volatility distribution comparison for organic compounds detected by the Vocus AIM using nitrate, iodide, chloride, and ammonia ion chemistries. Ion intensity represents the cumulative signal recorded for each ion chemistry. The background colors represent the saturation concentration (C_{sat}) in the range of ultra-low volatility (ULVOCs), extremely low volatility (ELVOCs), low volatility (LVOCs), semi-volatile (SVOCs), intermediate volatility (IVOCs), and volatile organic compounds (VOCs, pink). The pie charts represent the corresponding contributions of VOC, IVOC, SVOC, LVOC, ELVOC, and ULVOC classes from the O_3/OH initiated oxidation of α -pinene.